Available online at www.sciencedirect.com
ScienceDirect
Trans. Nonferrous Met. Soc. China 32(2022) 2866−2876
Transactions of Nonferrous Metals Society of China
www.tnmsc.cn

Simultaneous improvement in strength and ductility of extruded Mg alloy via novel closed forging extrusion

Kun-ming ZHANG[1], Chen QIN[1], Jia SHE[1,2], Xue-rui JING[1],
Peng PENG[3], Ai-tao TANG[1,2], Muhammad RASHAD[4,5], Fu-sheng PAN[1,2,3]

1. College of Materials Science and Engineering, Chongqing University, Chongqing 400044, China;
2. National Engineering Research Center for Mg Alloys, Chongqing University, Chongqing 400044, China;
3. School of Metallurgy and Materials Engineering,
Chongqing University of Science and Technology, Chongqing 401331, China;
4. Bernal Institute, Department of Chemical Sciences, University of Limerick, Limerick, V94 T9PX, Ireland;
5. School of Materials Science and Engineering,
Jiangsu University of Science and Technology, Zhenjiang 212003, China

Received 9 August 2021; accepted 3 March 2022

Abstract: A novel continuous plastic process employed on AZ31 Mg alloy called closed forging extrusion (CFE) was presented. The optical microscopy, scanning electron microscopy, electron back-scatter diffraction and tensile and compressive tests were employed to investigate the microstructure evolution and strengthening mechanism. The results indicated that the CFE-process can promote dynamic recrystallization (DRX), eliminate the coarsen unDRXed grain regions, refine the grains effectively, and improve the strength, plasticity and anisotropy of the alloy. The grain refinement was mainly attributed to the stress, which facilitated the nucleation of recrystallization and refined the microstructure via the CFE. The fully DRXed ultrafine grained structure improved the strength and plasticity simultaneously. After 60 s closed forging and continuous extrusion, the alloy exhibits relatively high TYS, UTS, CYS, elongation and yield asymmetry of 305 MPa, 337 MPa, 295 MPa, 27% and 0.97, respectively.
Key words: Mg alloys; extrusion; mechanical properties

1 Introduction

In recent decades, Mg alloys have gained more and more research attention as a promising structural material with respect of their excellent stiffness, special strength and low density [1,2]. At room temperature, unlike other alloys with face-centered, cubic structure or body-centered cubic structure, Mg alloys with a hexagonal close packed structure have not enough active systems to accommodate the deformation, which causes the poor formability and plasticity [3]. Meanwhile, the strong basal texture will form after plasticity process, which leads to heavy mechanical anisotropy and thus restricts the application of wrought Mg alloys [4]. Developing high strength, ductility and low anisotropy wrought is very crucial.

Dynamic recrystallization (DRX) usually occurs during the thermomechanical process of Mg alloys at elevated temperatures, which is an important mechanism for the workability and refine grains [5]. One DRX, named discontinuous dynamic recrystallization (DDRX), is made up of two stages: nucleation at serrated high angle grain boundaries

Corresponding author: Jia SHE, Tel: +86-18002325053, E-mail: jiashe@foxmail.com; Ai-tao TANG, E-mail: tat@cqu.edu.cn; Muhammad RASHAD, E-mail: rashadphy87@gmail.com
DOI: 10.1016/S1003-6326(22)65989-2

(HAGBs) by bulging and grain growth through grain boundaries migration [6]. The other DRX is continuous dynamic recrystallization (CDRX) according to the classified standard of nucleation and growth characteristics. CDRX is a process, which involves the absorption of dislocation in low angle grain boundaries (LAGBs), transformation of LAGBs to HAGBs and thus formation of new DRXed grains [6]. No matter what mechanism happens during the thermomechanical process, DRX has an effect on microstructural development and final properties of Mg alloys. For instance, the strong basal texture and coarse unDRXed grains formed after extrusion will cause heavy anisotropy [7].

Many attempts have been done to reduce the unDRXed field and refine grains. ZHENG et al [8] has successfully obtained the fully recrystallized ultrafine grained structure with an average grain size of about 100 nm by conducting the high pressure torsion (HPT) process on Mg−Zn−Zr−Ca alloy. They found that compared to the as-solution treated specimen, the yield strength is greatly enhanced from (107±4) to (311±3) MPa and the grain size is reduced from 570 to 100 nm after the HPT process by 360º rotation. However, the tensile ductility is sharply dropped from (13.9±0.5)% to (1.2±0.1)% before subsequent annealing at 300 °C for 1 min. KIM et al [9] found that DRX in the high temperature extrusion develops more completely than it does in the low temperature extrusion through studying ZK60 Mg alloy. However, for the specimen extruded at 180 °C with the average grain size of 1.9 μm, the yield strength is 53 MPa higher than that of extruded specimen at 290 °C with an average grain size of 8.2 μm, which is caused by grain growth at elevated temperatures. ZHOU et al [10] reported that plenty of second phase particles, such as *W*-$Mg_3Y_2Zn_3$ phase at grain boundaries and $MgZn_2$ phase in grains, exit in the microstructure due to the addition of Y and Zn in Mg−4.3Li−4.1Zn−1.4Y alloy, which easily promotes inhomogeneous nucleation of DRXed grains on the basis of particle-stimulated nucleation (PSN) mechanism. Generally, removing unDRXed regions can weaken the basal texture, refine grains, improve anisotropy, and finally enhance the overall performance. Those methods can be summarized as follows.

(1) Alloying: Alloy elements dissolved in the matrix increase the storage energy of deformed metal and hinder the grain boundary movement to refine the grains [11−13].

(2) Controlling temperature: The nucleation and growth of DRXed nucleus need diffusion of atoms [14]. The actual heated temperature must be greater than DRXed temperature, which can induce the operation of DRX process [15]. Nevertheless, too high heated temperature will cause to form the coarsen DRXed grains, and therefore it is very critical to control temperature parameter during deformation.

(3) Increasing plastic strain: It is well known that the reduction in storage energy is the driving force inducing DRX process. The larger the degree of deformation, the more the storage energy is, and the greater the driving force becomes [16,17].

Accumulative roll bonding (ARB) [18,19], cyclic extrusion compression (CEC) [20,21], high-pressure torsion (HPT) [22,23] and several other plastic deformation methods have been applied to increasing the deformation, henceforth boosting the DRXed fraction and finally refining grain in Mg alloys [24,25]. In this work, a novel extrusion method called closed forging extrusion (CFE) was employed to the commercial AZ31 Mg alloy. The primary purpose of this work is to reduce unDRXed regions, refine DRXed grains based on the increase of nucleation rate, and thereby improving the mechanical properties of final alloy.

2 Experimental

The raw material used in this work is as-cast Mg−3.18Al−1.00Zn−0.06Mn(wt.%), termed as AZ31 Mg alloy. Cylindrical billets with size of 80 mm in diameter and 50 mm in height were prepared for extrusion at 300 °C using direct extrusion under a ram rate of 1.0 m/min and an extrusion ratio of 20:1. There are some differences between the extrusion method used in this work and the conventional direct extrusion method. In this work, the extrusion die exit was firstly plugged using a baffle without hole to make the extrusion container as a closed space. When the extruded pressure reached 20 MPa, the samples were forged for 20 and 60 s respectively. Then the traditional positive extrusion was applied after using a mold with a hole to replace the baffle. The schematic diagram of closed forging extrusion is shown in

Fig. 1. Like the samples, the baffle and the mold were preheated at 300 °C. The extruded samples were defined as S0, S20 and S60 respectively with respect to forging holding time at 20 MPa. The sample of S0 was directly extruded without holding at 20 MPa. The novel processing method can be defined as closed forging extrusion.

Specimens for microstructural observation were cut from extruded bar with the size of 16 mm in diameter and ground with 400#, 800#, 1000#, and 2000# SiC grit papers. The specimens for optical microscope (OM) were etched with a corrosive mixture liquid containing 0.85 g picric acid, 2 mL glacial acetic acid, 4 mL water, and 14 mL alcohol after grinding.

Specimens for electron back-scatter diffraction (EBSD) test were prepared by electro-polishing at 20 V and −20 °C for 35 s using AC_2 solution and then the EBSD test was conducted on a JEOL 7800F field-emission scanning electron microscope, using a scan step-size of 0.2 μm. The size of specimens for EBSD observation was 3 mm × 5 mm × 7 mm in which the plane of 3 mm × 5 mm perpendicular to extrusion direction (ED) was observed.

Mechanical properties of the extruded alloy were characterized by compression and tension tests. For the tension tests, tension specimens were prepared with the size of 25 mm in gage length and cross section of 6 mm × 3 mm. The specimens used for the compression tests were 6 mm in diameter and 9 mm in height. Tensile and compress tests were implemented at an initial strain rate of 1.5×10^{-3} s^{-1}.

3 Results

3.1 Microstructures of extruded alloys

Figure 2 shows the OM image of the sample before extrusion. The alloy consists of dendrites, which is typical of the microstructure of as-cast Mg alloys. Figure 3 shows the optical micrographs of S0, S20 and S60 AZ31 alloys from the center to edge. It can be observed in Fig. 3(a) that the S0 sample consists of many coarse grains and fine equiaxed grains, representing the incomplete DRX. The unDRXed fraction is ~47% and the maximum of coarsen unDRXed grain size is ~1 mm. With the increase of forging time at a pressure of 20 MPa before extrusion, the grains of extruded alloys are refined and unDRXed regions are apparently reduced to ~8%, as shown in Fig. 3(b), corresponding to the extruded S20 sample. In S60 sample, the grains are significantly refined and the unDRXed field decreases to 5%. It can be noted that the closed forging process before extrusion can reduce unDRXed regions, promoting the DRX process and thus refining the grains.

The inverse pole figure (IPF) maps and textures are obtained from cross-sectional planes by conducting EBSD method on the three different samples, as shown in Fig. 4. The low angle grain boundaries (LAGBs), misorientation between 2° and 10°, are indicated by white lines, and the high angle grain boundaries (HAGBs), misorientation above 10°, are marked by black lines. The textures are displayed by (0001) pole figures of the S0, S20 and S60 samples, respectively. There are some coarse grains and fine DRXed grains in S0 sample with the average grain size of 2.34 μm, which is consistent with the former OM observation. Meanwhile, plenty of LAGBs can be observed within the coarse grains. The blue coarse grains are believed as unDRXed structures. In addition, the structure remains fine grain size ranging from 1.89 μm in S20 to 1.74 μm in S60 and more DRXed grains form. The DRX fraction is ~50% in S0 and finally goes up to ~98% in S60.

From the corresponding (0001) pole figures of samples, it can be observed that the maximal texture intensity is remarkably weakened from 9.01 to 3.75 with the prolongation of forging time at the

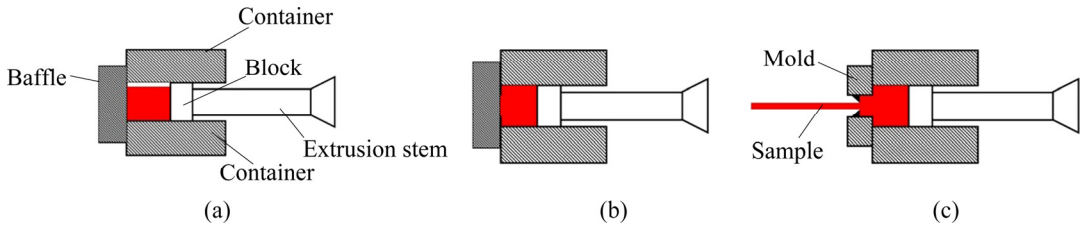

Fig. 1 Schematic diagram of closed forging extrusion

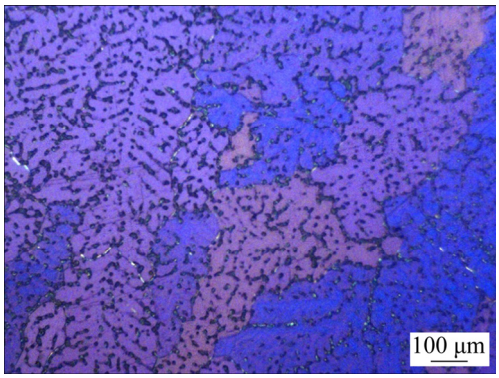

Fig. 2 OM image of as-cast sample

certain pressure prior to extrusion. Meanwhile, the shapes of pole figure also change with different holding time, from the typical ring-shaped texture at the beginning to an increasingly random texture [26]. The unDRXed area generally has a very strong basal texture [27], and thus reducing the unDRXed area can weaken the basal texture [13]. The treatment of closed forging process prior to extrusion significantly reduces the unDRXed area of the alloy, promotes the recrystallization, and finally not only refines the grains but also weakens the basal texture.

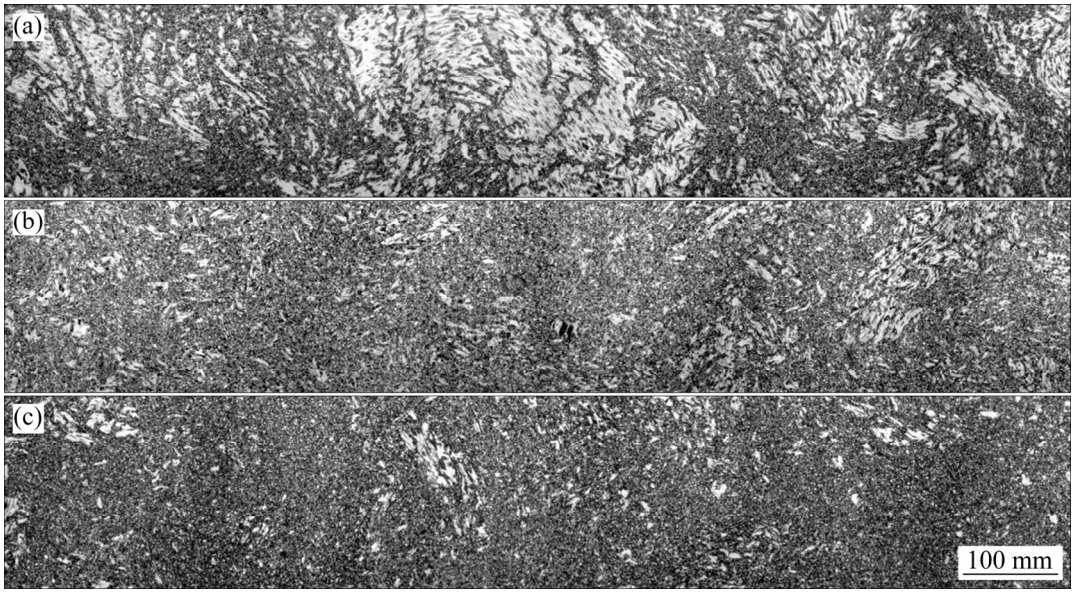

Fig. 3 Microstructures of extruded alloys: (a) S0; (b) S20; (c) S60

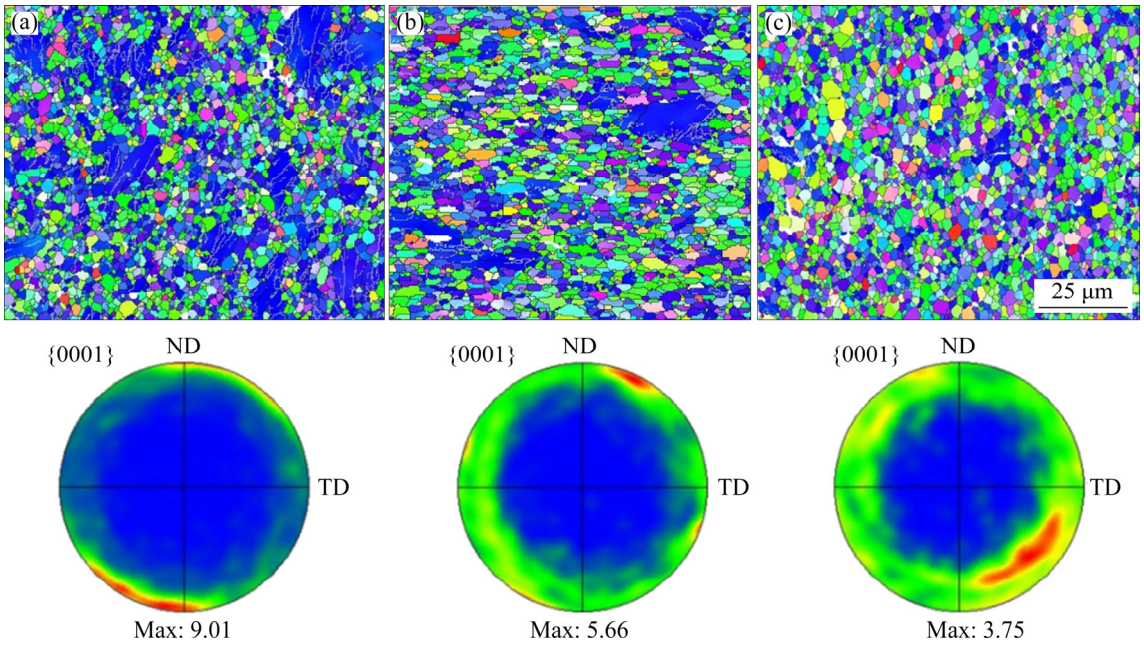

Fig. 4 Inverse pole figure (IPF) maps and corresponding (0001) pole figure: (a) S0; (b) S20; (c) S60

3.2 Mechanical properties

The tension and compression stress−strain curves of the extruded samples at room temperature are shown in Fig. 5. The detailed numerical values of mechanical properties obtained from the curves are shown in Table 1. For the specimen S0, the tensile yield stress (TYS), ultimate tensile strength (UTS), and fracture elongation (σ) are ~309 MPa, ~341 MPa, and ~19%, respectively. Compared to S0, the TYS and UTS of the S20 decrease by ~18 MPa and ~11 MPa, respectively. Severally, while the fracture elongation increases from 19% to 25%. The S60 sample exhibits relatively high TYS and fracture elongation of ~305 MPa and ~27%, respectively. From the compressive stress−strain curves, the compressive yield strength (CYS) increases with the prolongation of holding time. The compressive yield strength of S60 sample is 295 MPa, which is about 40 MPa higher than that of S0 sample. In addition, the values of yield asymmetry ($\sigma_{CYS}/\sigma_{TYS}$) of S0 also rise from 0.83 to 0.97 (for S60), indicating that yield asymmetry is improved. Totally, the sample S60 represents the best combination of elongation and tension−compression yield asymmetry. Yield strength and tensile failure strains of typical severe plastic deformation AZ31 alloys, including present CFE samples, conventional extrusion [33,34], and the reported SPD AZ31 alloys including ECAP [10], CEC [14] and DSR [13,35], have been compared as shown in Fig. 5(c). The comparison shows that the present CFE AZ31 alloys via PFE-process are in a region of high yield strength and elongation.

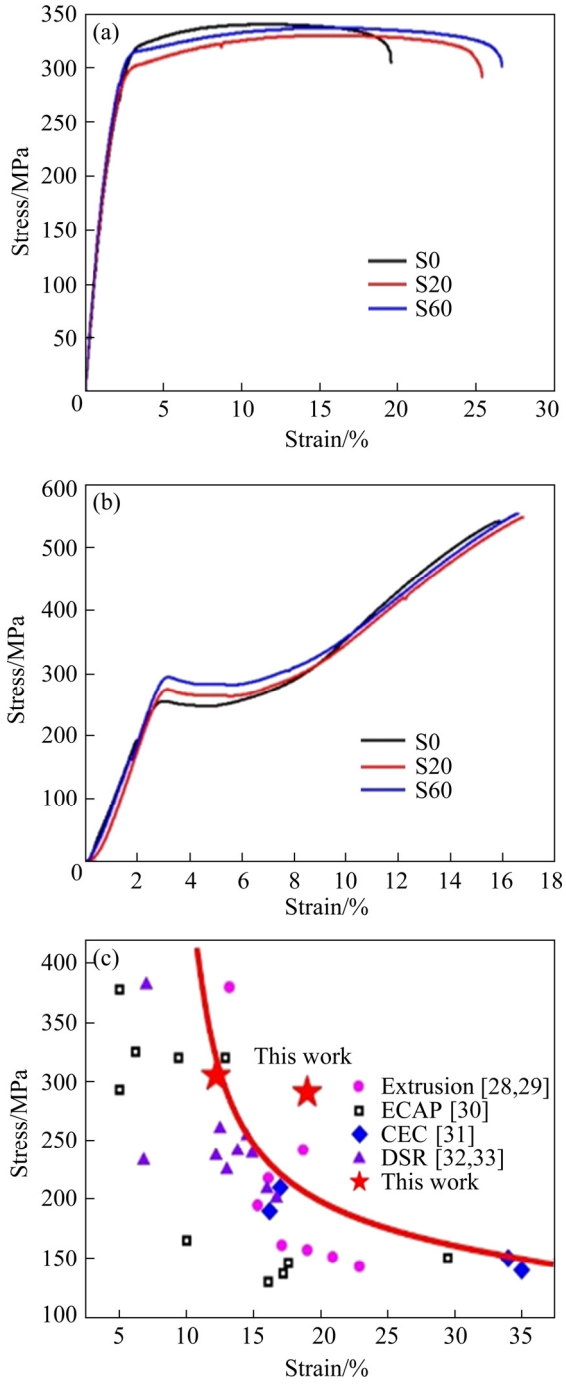

Fig. 5 Tensile engineering stress−strain curves (a), compressive engineering stress−strain curves (b), and yield stress−strain curves (c)

Table 1 Mechanical properties and yield asymmetry of extruded samples

Sample	TYS/ MPa	UTS/ MPa	CYS/ MPa	δ/%	$\sigma_{CYS}/\sigma_{TYS}$
S0	309	341	256	19	0.83
S20	291	330	275	25	0.94
S60	305	337	295	27	0.97

4 Discussion

4.1 Microstructure evolution

In order to clarify the microstructural evolution during CFE, the interrupted extrusion method based on the closed forging process of holding time at 20 MPa before extrusion was conducted on AZ31 alloy in this work. The interrupted extruded samples were defined as IS0 and IS60 according to the holding forging time of 0 and 60 s, respectively.

Figure 6(a) shows the schematic diagram of the interrupted extrusion samples on central section parallel to the ED. The microstructure observations of the interrupted extrusion samples were carried out at different locations below the extrusion die, as

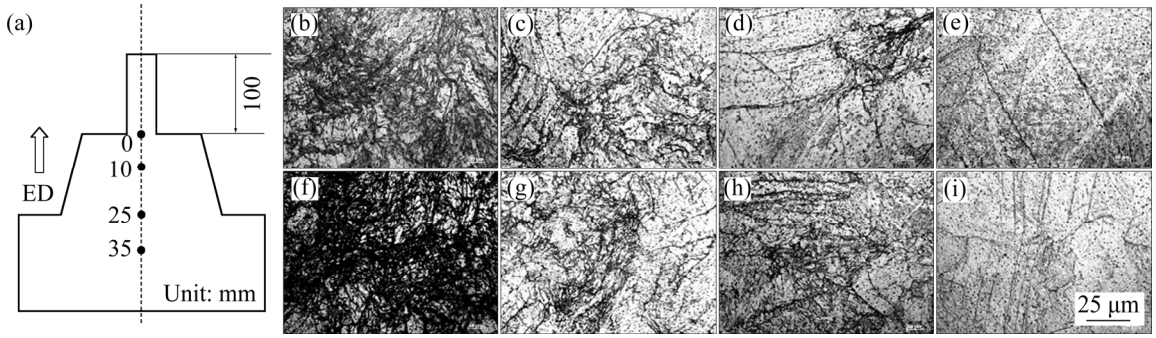

Fig. 6 Schematic diagram of microstructure observation locations for interrupted extrusion samples on central section parallel to ED (a), and microstructures of interrupted extrusion samples at different locations below extrusion die: (b) IS0-0; (c) IS0-10; (d) IS0-25; (e) IS0-35; (f) IS60-0; (g) IS60-10; (h) IS60-25; (i) IS60-35

presented by black dots, combined with OM and EBSD method. Figures 6(b−i) show the microstructures of the IS0 and IS60 at different locations below the extrusion die, respectively. A few lenticular twin-like morphologies are observed in IS0-35 due to the small degree of deformation gained at the locations away from the extrusion die. With further deformation, as the twins disappear, more and more shear bands can be found at 25 mm. At 10 mm, the new DRXed grains conspicuously increase and finer DRXed grains form, leading to the development of a typical bimodal microstructure consisting of fine DRXed and coarse unDRXed grains with further deformation at 0 mm. In other words, the unDRXed regions gradually decrease from the location of 35 mm to that of 0 mm due to the fact that the locations closer to the extrusion die present encounter greater deformation, as shown in Figs. 6(b−e), respectively. Notably, compared to the samples of IS0, more fine gains form along the boundaries at the same observed location in IS60, which indicates the further development of DRX process. Undoubtedly, it is the treatment of closed forging process before extrusion that accelerates the DRX process in this work.

The EBSD results of the interrupted extrusion samples are shown in Fig. 7. At 25 mm in IS0 sample (Fig. 7(a)), a few lenticular twin-like morphologies and fine grains can be observed. In addition, most of fine grains nucleate along the HAGBs, while several grains form within the original deformed grains and along the twin boundaries, which demonstrate the operations of DDRX process and twin-induced DRX process. The same coarsen deformed grain presents different colors marked in IPF map, uncovering the continuous orientation change of unDRXed grains. Meanwhile, combined with Fig. 7(b), it can be intuitively observed that some complete DRXed grains and subgrains form within the deformed grains, amply manifesting that CDRX mechanism occurs in this case. Compared with IS0, finer DRXed gains are found in IS60 (Fig. 7(d)), which is in conformity with former OM observation. More HAGBs as well as LAGBs are found and the majorities of fine DRXed grains nucleate and grow at serrated pre-existing HAGBs by bulging, which can adequately demonstrate the operation of DDRX process in IS60. With further straining, most of LAGBs resulting from the accumulation of dislocation in the deformed structure can transform into HAGBs due to trapping of dislocation. Finally, making subgrains into new DRXed grains can be also proved by Fig. 4.

The distribution of local stain concentration for interrupted extrusion samples is characterized by the kernel average misorientation (KAM) maps [34], as shown in Figs. 7(c) and (f). The KAM maps reveal that the high local remaining strain mainly concentrates on the HAGBs, which stores a large amount of energy to facilitate the nucleation and growth of DRXed grains. The higher proportion of high local strain is observed with the prolongation of holding time starting from 20 MPa in IS60, indicating that more DRXed grains will form along the boundaries. Meanwhile, the regional stress in the recrystallization nucleation has been released, as shown in blue in Fig. 7(f). As the extrusion processing goes on, IS60 will undergo more dynamic recrystallization, thus forming a more uniform structure. It is difficult to obtain uniform recrystallization structure in IS0 due to

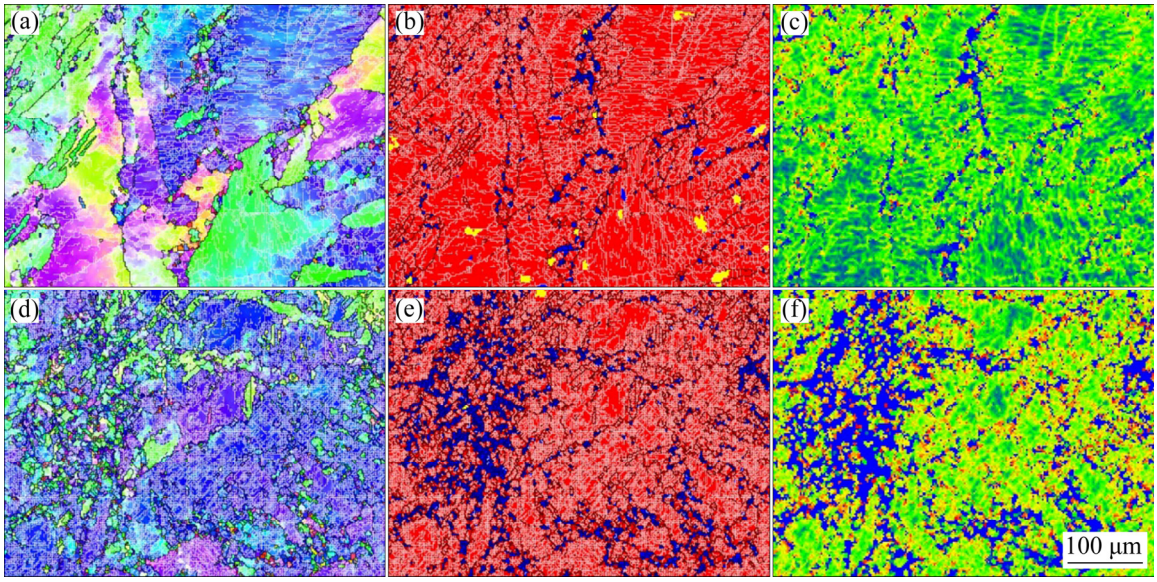

Fig. 7 EBSD results of interrupted extrusion samples at 25 mm below extrusion die: IPF maps of IS0 (a) and IS60 (d), DRX maps of IS0 (b) and IS60 (e), and KAM maps of IS0 (c) and IS60 (f)

insufficient recrystallization nucleation. The decreasing of unDRXed regions can weaken the texture, as shown in (0001) pole figures that the max intensity of texture decreases from 9.01 to 3.75. Apparently, compared to traditional positive extrusion, the greater stress can be gained via closed forging process before extrusion, which can facilitate the nucleation of recrystallization, accelerate the recrystallization process, and obtain uniform and fine structure.

4.2 Mechanical properties

It is well known that the unDRXed region owns hard orientation, which can make a positive contribution to the tensile yield strength [35]. Yield strength is related to the average gain size [36]. Besides, the yield strength is also associated with orientation of grains. The relationship can be expressed by [16]

$$\sigma_y = \tau_k / m$$

where σ_y is the yield strength, τ_k is the critical shear stress, and m is the orientation factor or schmid factor. The value of the critical shear stress depends on the crystal structure, purity, processing state, test temperature, and loading speed of the metal. When the conditions are constant, the critical shear stress of each crystal has a fixed value, regardless of the magnitude, direction, and mode of action of the external force. Thus, σ_y will change with orientation factor m. Slip is the easiest in metal when the orientation factor has a maximum value of 0.5, defined as soft orientation, while the crystal cannot slip at all when the orientation factor has a minimum value of 0, defined as hard orientation. In other words, greater σ_y is caused by the smaller orientation factor closer to 0, which means that large tensile stress is required for the crystal to operate slip and cause plastic deformation.

Figure 8 shows Schmid factor maps of the basal plane of extruded alloys. The most of coarse unDRXed grains present blue and the average SF is in S0 sample, indicating that the basal plane is difficult to slide due to the existence of many grains with hard orientation. The unDRXed regions owning the harder orientations are difficult to deform when performing a tensile test, which may lead to the larger tensile yield strength [37]. That is the reason why the tensile yield strength does not enhance, but minish although the average grain size reduces from S0 to S20 sample. With further straining, the yield strength is smaller than that of S0 and bigger than that of S20 and S60 samples with a view to the coefficient effect of unDRXed regions and average gain size. In addition, the fine grains with random orientations produce a high Schmid factor value and thus improve the ductility.

The previous experimental results as well as the analysis show that the extruded samples at 300 °C have high strength and the S60 sample has excellent overall performance. In this section, the theoretical contribution of various strengthening

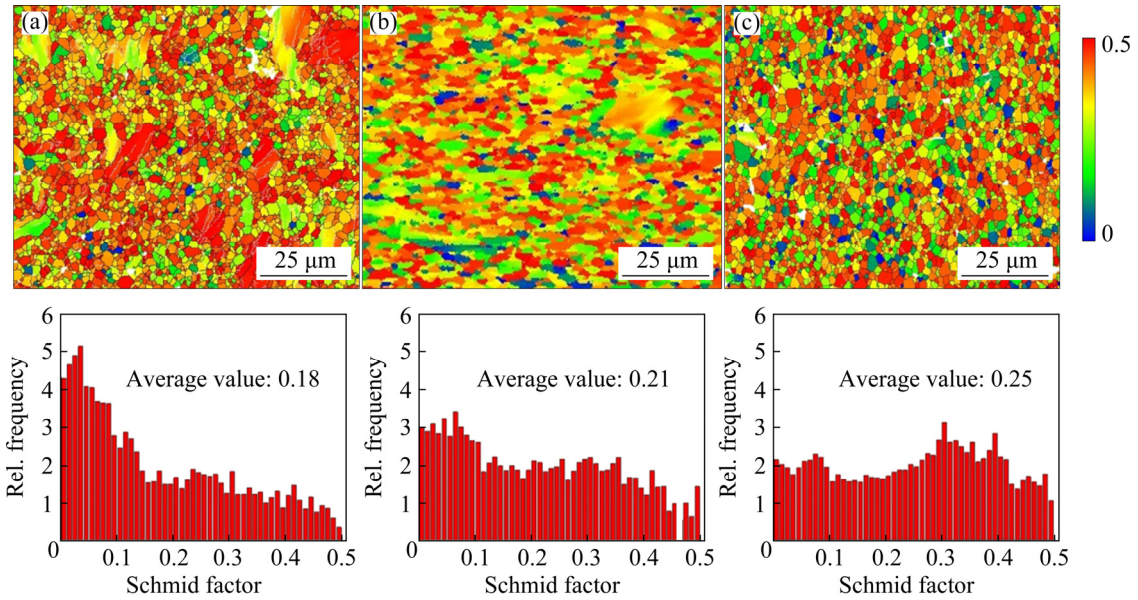

Fig. 8 Schmid factor maps of extruded alloys: (a) S0; (b) S20; (c) S60

mechanisms to the tensile yield strength of the extruded deformed samples at 300 °C will be calculated with specific values.

In extruded alloys, the main strengthening factors are grain size, residual dislocations, and uniformly distributed second-phase particles [38]. For a typical AZ31 commercial Mg alloy, few second-phase particles are generated during extrusion, and the contribution to the strength is negligible. As a result of the 60 s pre-die forging, the extruded alloy grains were significantly refined, making the contribution of grain size to strength significantly higher than that of the samples without the closed forging treatment. S60 samples had fewer coarse unDRXed regions, but their dislocation density was still higher than that of S0 sample, mainly because the pre-die forging for 60 s before extrusion introduced a larger strain and more dislocations were generated. However, the residual dislocation strength is related to the Schmidt factor and the undynamic recrystallization fraction in addition to the dislocation density inside the material, and these factors together lead to a higher contribution of residual dislocations to the strength in the S0 sample than that in the S20 and S60 samples.

In order to reveal the compression quality, the pre-compressed tests are conducted on the extruded alloys. Figure 9 shows the OM images of pre-compressed samples. We can see that, many tensile twins easily caused by pre-compression

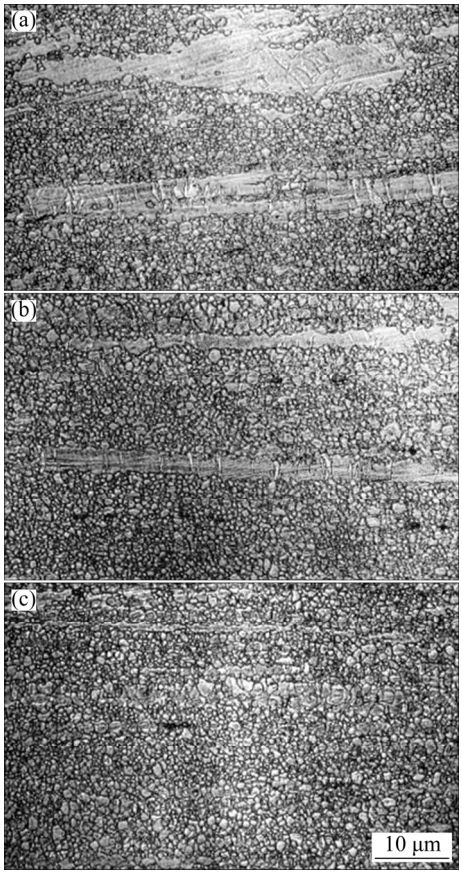

Fig. 9 OM images of pre-compressed alloys: (a) S0; (b) S20; (c) S60

along extrusion direction (ED) are observed within the unDRXed regions in S0 and reduce gradually with further the extension of closed forging time before extrusion. EBSD results of the unDRXed

grain are shown in Fig. 10. The unDRXed region with the lower SF is hard orientation indicated by blue color (Fig. 10(b)). The *c*-axis of the unDRXed region is perpendicular to the extrusion direction (Fig. 10(c)). Therefore, the *c*-axis is under tensile stress when the compressive stress is applied, which is very easy to generate tensile twins [39]. In other words, the operation of twin becomes very difficult with decrement of unDRXed region, which can promote the enhancement of compressive yield strength. The compressive yield strength is improved drastically in S60, caused by the effect of decrease in twin and average grain size. The S60 sample thus has a good overall performance in consideration of yield strength, ductility, and isotropy.

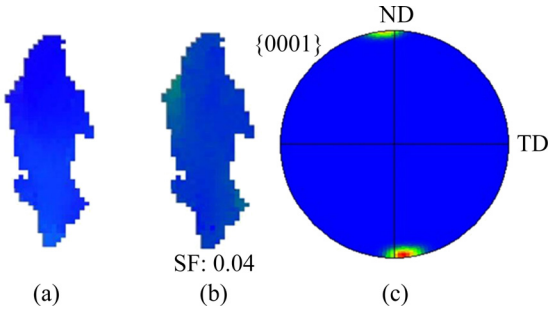

Fig. 10 EBSD results of unDRXed grain: (a) IPF map; (b) Schmid factor map; (c) (0001) pole figure

5 Conclusions

(1) After 60 s closed froging and continuous extrusion, the grains are significantly refined and the unDRXed field decreases to 5%. The average grain size of S60 sample is ~1.7 μm.

(2) The S60 sample exhibits relatively high TYS, UTS, CYS, elongation and yield asymmetry ($\sigma_{CYS}/\sigma_{TYS}$) of 305 MPa, 337 MPa, 295 MPa, 27%, and 0.97, respectively.

(3) The highly uniformed fine-grained structure of CFE is attributed to facilitate the nucleation of recrystallization, and accelerate the recrystallization process caused by the closed forging before extrusion.

Acknowledgments

This research was funded by the National Natural Science Foundation of China (Nos. 51971042, 51901028), the Fundamental Research Funds for the Central Universities Project, China (No. 2021CDJQY-038), and the Chongqing Academician Special Fund, China (Nos. cstc2018jcyj-yszxX0007, cstc2019yszx-jcyjX0004).

References

[1] SONG J F, SHE J, CHEN D L, PAN F S. Latest research advances on magnesium and magnesium alloys worldwide [J]. Journal of Magnesium and Alloys, 2020, 8: 1−41.

[2] DING Z B, ZHAO Y H, LU R P, YUAN M N, WANG Z L, LI H J, HOU H. Effect of Zn addition on microstructure and mechanical properties of cast Mg−Gd−Y−Zr alloys [J]. Transactions of Nonferrous Metals Society of China, 2019, 29(4): 722−734.

[3] LIU T T, YANG Q S, GUO N, LU Y, SONG B. Stability of twins in Mg alloys — A short review [J]. Journal of Magnesium and Alloys, 2020, 8(1): 66−77.

[4] WIESE B, WILLUMEITRÖMER R, LETZIG D, BOHLEN J. Alloying effect of silver in magnesium on the development of microstructure and mechanical properties by indirect extrusion [J]. Journal of Magnesium and Alloys, 2021, 9(1): 112−122.

[5] DING T, YAN H G, CHEN J H, XIA W J, SU B, YU Z L. Dynamic recrystallization and mechanical properties of high-strain-rate hot rolled Mg−5Zn alloys with addition of Ca and Sr [J]. Transactions of Nonferrous Metals Society of China, 2019, 29(8): 1631−1640.

[6] DU Y Z, LIU D J, GE Y F, JIANG B L. Effects of deformation parameters on microstructure and texture of Mg−Zn−Ce alloy [J]. Transactions of Nonferrous Metals Society of China, 2020, 30(10): 2658−2668.

[7] HOSEINI-ATHAR M M, MAHMUDI R, BABU R P, HEDSTRÖM P. Tailoring the texture of an extruded Mg sheet through constrained groove pressing for achieving low mechanical anisotropy and high yield strength [J]. Scripta Materialia, 2020, 186: 253−258.

[8] ZHENG R X, BHATTACHARJEE T, SHIBATA A, SASAKI T, HONO K, JOSHI M, TSUJI N. Simultaneously enhanced strength and ductility of Mg−Zn−Zr−Ca alloy with fully recrystallized ultrafine grained structures [J]. Scripta Materialia, 2017, 131: 1−5.

[9] KIM B, BAEK S M, LEE J G, PARK S S. Enhanced strength and plasticity of Mg−6Zn−0.5Zr alloy by low-temperature indirect extrusion [J]. Journal of Alloys and Compounds, 2017, 706: 56−62.

[10] ZHOU Y C, CHEN Z Y, JI J H, SUN Z J. Effects of second phases on deformation behavior and dynamic recrystallization of as-cast Mg−4.3Li−4.1Zn−1.4Y alloy during hot compression [J]. Journal of Alloys and Compounds, 2019, 770: 540−548.

[11] MAJD A M, FARZINFAR M, PASHAKHANLOU M, NAYYERI M J. Effect of RE elements on the microstructural and mechanical properties of as-cast and age hardening processed Mg–4Al–2Sn alloy [J]. Journal of Magnesium and Alloys, 2018, 6(3): 309−317.

[12] SHE J, PAN F S, GUO W, TANG A T, GAO Z X, LUO S Q, SONG K, YU Z W, RASHAD M. Effect of high Mn content on development of ultra-fine grain extruded magnesium alloy [J]. Materials & Design, 2016, 90: 7−12.

[13] SHE J, PAN F, ZHANG J, TANG A, LUO S, YU Z, SONG K, RASHAD M. Microstructure and mechanical properties of Mg–Al–Sn extruded alloys [J]. Journal of Alloys and Compounds, 2016, 657: 893−905.
[14] HOSEINI-ATHAR M M, MAHMUDI R, BABU R P, HEDSTRÖM P. Effect of Zn content on the microstructural stability and grain growth kinetics of fine-grained extruded Mg−Gd−Zn alloys [J]. Journal of Alloys and Compounds, 2020, 831: 154766.
[15] HADORN J P, HANTZSCHE K, YI S, BOHLEN J, LETZIG D, AGNEW S R. Effects of solute and second-phase particles on the texture of Nd-containing Mg alloys [J]. Metallurgical and Materials Transactions A, 2012, 43(4): 1363−1375.
[16] HUANG H, TANG Z B, TIAN Y, JIA G Z, NIU J L, ZHANG H, PEI J, YUAN G Y, DING W J. Effects of cyclic extrusion and compression parameters on microstructure and mechanical properties of Mg−1.50Zn−0.25Gd alloy [J]. Materials & Design, 2015, 86: 788−796.
[17] GUAN D K, RAINFORTH W M, GAO J H, SHARP J, WYNNE B, MA L. Individual effect of recrystallisation nucleation sites on texture weakening in a magnesium alloy: Part 1—Double twins [J]. Acta Materialia, 2017, 135: 14−24.
[18] SAITO Y, TSUJI N, UTSUNOMIYA H, SAKAI T, HONG R G. Ultra-fine grained bulk aluminum produced by accumulative roll-bonding (ARB) process [J]. Scripta Materialia, 1998, 39(9): 1221−1227.
[19] SAITO Y, UTSUNOMIYA H, TSUJI N, SAKAI T. Novel ultra-high straining process for bulk materials—Development of the accumulative roll-bonding (ARB) process [J]. Acta Materialia, 1999, 47(2): 579−583.
[20] WANG Q D, MU Y L, LIN J B, ZHANG L, ROVEN H J. Strengthening and toughening mechanisms of an ultrafine grained Mg−Gd−Y−Zr alloy processed by cyclic extrusion and compression [J]. Materials Science and Engineering: A, 2017, 699: 26−30.
[21] ZHANG L X, ZHANG W C, CAO B, CHEN W Z, DUAN J P, CUI G R. Effects of texture and grain size on the yield strength of ZK61 alloy rods processed by cyclic extrusion and compression [J]. Materials, 2017, 10(11): 1234.
[22] SUN W J, QIAO X G, ZHENG M M, HU N, GAO N, STARINK M J. Evolution of long-period stacking ordered structure and hardness of Mg−8.2Gd−3.8Y−1.0Zn−0.4Zr alloy during processing by high pressure torsion [J]. Materials Science and Engineering A, 2018, 738: 238−252.
[23] TANG L L, ZHAO Y H, LIANG N N, ISLAMGALIEV R K, VALIEV R Z, ZHU Y. Localized deformation via multiple twinning in a Mg−Gd−Y−Zr alloy processed by high-pressure torsion [J]. Materials Science and Engineering A, 2016, 677: 68−75.
[24] LEE J H, KWAK B J, KONG T, PARK S H, LEE T. Improved tensile properties of AZ31 Mg alloy subjected to various caliber-rolling strains [J]. Journal of Magnesium and Alloys, 2019, 7(3): 381−387.
[25] LIU H, JU J, BAI J, SUN J P, SONG D, YAN J L, JIANG J H, MA A B. Preparation, microstructure evolutions, and mechanical property of an ultra-fine grained Mg−10Gd−4Y−1.5Zn− 0.5Zr alloy [J]. Metals, 2017, 7(10): 398.
[26] JIANG M G, YAN H, GAO L, CHEN R S. Microstructural evolution of Mg−7Al−2Sn Mg alloy during multi-directional impact forging [J]. Journal of Magnesium and Alloys, 2015, 3(3): 180−187.
[27] HAO M J, CHENG W L, WANG L F, MOSTAED E, BIAN L P, WANG H X, NIU X F. Texture evolution in Mg−8Sn−1Zn−1Al alloy during hot compression via competition between twinning and dynamic precipitation [J]. Materials Science and Engineering: A, 2019, 748: 418−427.
[28] ZENG Z R, ZHU Y M, LIU R L, XU S W, DAVIES C H J, NIE J F, BIRBILIS N. Achieving exceptionally high strength in Mg−3Al−1Zn−0.3Mn extrusions via suppressing intergranular deformation [J]. Acta Materialia, 2018, 160: 97−108.
[29] XU J, YANG T H, JIANG B, SONG J F, HE J J, WANG Q H, CHAI Y F, HUANG G S, PAN F S. Improved mechanical properties of Mg−3Al−1Zn alloy sheets by optimizing the extrusion die angles: Microstructural and texture evolution [J]. Journal of Alloys and Compounds, 2018, 762: 719−729.
[30] ZHAO G W, FAN J F, ZHANG H, ZHANG Q, YANG J, DONG H B, XU B S. Exceptional mechanical properties of ultra-fine grain AZ31 alloy by the combined processing of ECAP, rolling and EPT [J]. Materials Science and Engineering: A, 2018, 731: 54−60.
[31] CHEN Y J, WANG Q D, ROVEN H J, LIU M P, KARLSEN M, YU Y D, HJELEN J. Network-shaped fine-grained microstructure and high ductility of magnesium alloy fabricated by cyclic extrusion compression [J]. Scripta Materialia, 2008, 58: 311−314.
[32] FU H, GE B C, XIN Y C, WU R Z, FERNANDEZ C, HUANG J Y, PENG Q M. Achieving high strength and ductility in magnesium alloys via densely hierarchical double contraction nanotwins [J]. Nano Letters, 2017, 17: 6117−6124.
[33] KO Y G, HAMAD K. Structural features and mechanical properties of AZ31 Mg alloy warm-deformed by differential speed rolling [J]. Journal of Alloys and Compounds, 2018, 744: 96−103.
[34] PENG P, SHE J, TANG A T, ZHANG J Y, ZHOU S B, XIONG X, PAN F S. Novel continuous forging extrusion in a one-step extrusion process for bulk ultrafine magnesium alloy [J]. Materials Science and Engineering A, 2019, 764: 138144.
[35] LI Z T, QIAO X G, XU C, KAMADO S, ZHENG M Y, LUO A A. Ultrahigh strength Mg−Al−Ca−Mn extrusion alloys with various aluminum contents [J]. Journal of Alloys and Compounds, 2019, 792: 130−141.
[36] PENG P, HE X, SHE J, TANG A T, RASHAD M, ZHOU S B, ZHANG G, MI X X, PAN F S. Novel low-cost magnesium alloys with high yield strength and plasticity [J]. Materials Science and Engineering: A, 2019, 766: 138332.
[37] SHE J, PENG P, XIAO L, TANG A T, WANG Y, PAN F S. Development of high strength and ductility in Mg−2Zn extruded alloy by high content Mn-alloying [J]. Materials Science and Engineering A, 2019, 765: 138203.
[38] DU Y Z, QIAO X G, ZHENG M Y, WU K, XU S W. Development of high-strength, low-cost wrought Mg–2.5mass%Zn alloy through micro-alloying with Ca and La [J]. Materials & Design, 2015, 85: 549−557.
[39] XIN Y C, ZHOU H, YU H H, HONG R, ZHANG G H, LIU Q. Controlling the recrystallization behavior of a Mg–3Al–1Zn alloy containing extension twins [J]. Materials Science and Engineering A, 2015, 622: 178−183.

封闭锻造挤压镁合金同步提高强度和塑性

张坤敏[1]，秦 晨[1]，佘 加[1,2]，敬学锐[1]，彭 鹏[3]，汤爱涛[1,2]，Muhammad RASHAD[4,5]，潘复生[1,2,3]

1. 重庆大学 材料科学与工程学院，重庆 400044；
2. 重庆大学 国家镁合金材料工程技术研究中心，重庆 400044；
3. 重庆科技大学 冶金与材料工程学院，重庆 401331；
4. Bernal Institute, Department of Chemical Sciences, University of Limerick, Limerick, V94 T9PX, Ireland；
5. 江苏科技大学 材料科学与工程学院，镇江 212003

摘 要：介绍一种用于 AZ31 镁合金的新型连续塑性工艺，即闭式锻造挤压。采用光学显微镜、扫描电子显微镜、电子背散射衍射和拉伸和压缩试验研究合金微观结构的演变和强化机制。结果表明，该工艺可以促进动态再结晶，消除粗大的未动态再结晶晶粒区域，有效细化晶粒，并提高合金的强度、塑性和各向异性。晶粒细化主要归功于应力，促进再结晶的形核并细化组织。完全再结晶的超细晶组织同时提高了强度和塑性。经过 60 s 封闭锻造和连续挤压后，合金表现出较高的力学性能，其拉伸屈服强度、抗拉强度、抗压强度、伸长率和屈服不对称性分别为 305 MPa、337 MPa、295 MPa、27%和 0.97。

关键词：镁合金；挤压；力学性能

(Edited by Xiang-qun LI)